Manuscript prepared for Ocean Sci. Discuss.
with version 2014/09/16 7.15 Copernicus papers of the LaTeX class copernicus.cls.
Date: 11 November 2015

Impact of variable sea-water conductivity on motional induction simulated with an OGCM

C. Irrgang[1,2], **J. Saynisch**[1], **and M. Thomas**[1,2]

[1]Helmholtz Centre Potsdam, GFZ German Research Centre for Geosciences, Section 1.3, Earth System Modelling, Potsdam, Germany
[2]Freie Universität Berlin, Institute of Meteorology, Berlin, Germany

Correspondence to: C. Irrgang (irrgang@gfz-potsdam.de)

Abstract

Carrying high concentrations of dissolved salt, ocean water is a good electrical conductor. As sea-water flows through the Earth's ambient geomagnetic field, electric fields are generated, which in turn induce secondary magnetic fields. In current models for oceanic induced magnetic fields, a realistic consideration of sea-water conductivity is often neglected and the effect on the variability of the oceanic induced magnetic field unknown. To model magnetic fields that are induced by non-tidal global ocean currents, an electromagnetic induction model is implemented into the Ocean Model for Circulation and Tides (OMCT). This provides the opportunity to not only model oceanic induced magnetic signals, but to assess the impact of oceanographic phenomena on the induction process. In this paper, the sensitivity of the induction process due to spatial and temporal variations in sea-water conductivity is investigated. It is shown that assuming an ocean-wide uniform conductivity is insufficient to accurately capture the temporal variability of the magnetic signal. Using instead a realistic global sea-water conductivity distribution increases the temporal variability of the magnetic field up to 45 %. Especially vertical gradients in sea-water conductivity prove to be a key factor for the variability of the oceanic induced magnetic field. However, temporal variations of sea-water conductivity only marginally affect the magnetic signal.

1 Introduction

The principle of electromagnetic induction due to water flow is long known and was first described by Faraday (1832). As the oceans move through the Earth's ambient geomagnetic field, salt-ions in ocean water are deflected by the Lorentz force. Thereby, spatial accumulations of electric charge are formed, leading to the generation of electric currents, which in turn induce secondary magnetic fields. This process is often referred to as "motional induction". Fundamental theoretical work in the modern investigation of ocean generated electric fields was done by Larsen (1968) and Sanford (1971). Chave (1983) discussed electromagnetic induction due to ocean dynamics, as well as the effects of coastlines and

the electrical structure of the Earth. With the advance in computational power, ocean models and data have been used in studies to estimate motionally induced magnetic signals. Stephenson and Bryan (1992); Tyler et al. (1997) and Manoj et al. (2006) focused on motional induction due to global ocean circulation, while Tyler et al. (2003); Kuvshinov et al. (2006); Dostal et al. (2012) and Schnepf et al. (2014) discussed the modelling and observation of electromagnetic fields due to ocean tides. Flosadóttir et al. (1997) and Vivier et al. (2004) investigated electromagnetic fields on a regional scale, focusing on the North Atlantic circulation and the Antarctic Circumpolar Current. A comprehensive review of modelling electromagnetic induction in the ocean was conducted by Kuvshinov (2008). Despite the varying research focus of these studies on different oceanographic processes and spatio-temporal scales, there is a consensus regarding the small variability of the oceanic induced magnetic field and its difficult detectability and separability from other magnetic signals in satellite data. In many regions, the crustal magnetic field has comparable or higher amplitudes in satellite measurements which makes it challenging to separate both contributions (Kuvshinov, 2008). The temporal variability of the oceanic induced magnetic field, however, distinguishes it from the static crustal field.

In the above mentioned studies, sea-water conductivity is treated in different ways. Both homogeneous and inhomogeneous sea-water conductivity distributions are used. In addition, sea-water conductivity is assumed either constant or variable in time. Most often, a globally uniform value is used instead of a realistic conductivity distribution in the ocean. Sea-water conductivity can be derived from salinity and temperature, where the temperature is the predominant component. Both exhibit large spatial variations in the ocean and evolve in time. The typical mean conductivity of sea-water lies in the range of 3–4 $\mathrm{S\,m^{-1}}$. Strongest changes in sea-water conductivity occur above the main thermocline, with highest values reaching up to 6 $\mathrm{S\,m^{-1}}$. Chave and Luther (1990) investigated the effect of vertically varying sea-water conductivity on low-frequency, motionally induced electromagnetic fields on a theoretical basis, considering different one-dimensional vertical conductivity profiles. The influence of a realistic three-dimensional and time-varying sea-water conductivity on

the variability of magnetic fields which are induced by the ocean global circulation is still unknown.

The aim of this study is to examine the spatial and temporal influence of sea-water conductivity on the variability of the motionally induced magnetic field in the framework of an ocean global circulation model. This allows to answer the question whether it is necessary to account for a realistic sea-water conductivity distribution in the ocean and which simplifications are justifiable in order to capture the variability of the magnetic field accurately. Therefore, an electromagnetic induction model is coupled to an ocean global circulation model. The two models and the experiment setup are described in Sect. 2 of this paper. In Sect. 3, the results are presented and discussed. In Sect. 4, the conclusions are drawn and a summary is given.

2 Methodology

2.1 Global ocean model

The Ocean Model for Circulation and Tides (OMCT, Thomas et al., 2001; Dobslaw and Thomas, 2007) is used to model and simulate the global ocean circulation. The model is based on non-linear balance equations for momentum, the continuity equation, and conservation equations for heat and salt. In our configuration, the baroclinic ocean global circulation model (OGCM) uses a horizontal resolution of $1.875^\circ \times 1.875^\circ$, 13 layers in the vertical and a time-step of 30 min. The hydrostatic and the Boussinesq approximations are applied, whereas the correction of artificial mass change due to the Boussinesq approximation follows Greatbatch (1994). Tidal flows are not considered in this configuration, as the focus lies solely on global circulation patterns. To generate a realistic distribution and temporal variability of sea-water conductivity and ocean velocities, the model is forced with heat-flux, wind-stress, surface-pressure, precipitation and evaporation, which are based on 6 hourly ERA-Interim products from the European Centre for Medium-Range Weather Forecasts (ECMWF, Dee et al., 2011). Additionally, the model is forced with daily river-runoff from the

Land Surface Discharge Model (LSDM, Dill, 2008) which is also forced by the ECMWF-Interim data.

In this configuration, the OMCT realistically resolves the main features of ocean global circulation, e.g., the Antarctic Circumpolar Current and Western Boundary Currents (see Sect. 3 and Dobslaw and Thomas (2007), esp. Figs. 6 and 7). Eddies and other small-scale features are not resolved by the current configuration of the OMCT. These features have a considerable effect on the motionally induced magnetic field at sea-surface. Due to the smoothing effect of the upwardly continuation to satellite altitude, however, the small-scale features are neither visible in the spatial pattern of the magnetic signal at satellite altitude nor affecting the estimated strength of the magnetic signal (Vennerstrom et al., 2005). In the present study, the focus lies therefore on large-scale ocean global circulation patterns that predominantly characterize the oceanic induced magnetic signal at both sea-surface and satellite altitude. Nevertheless, the findings of the experiments in this study are applicable to both eddy-resolving models and models of tidal motion.

2.2 Electromagnetic induction model

The electromagnetic induction model is based on a 2-D induction equation and follows the same model approach as Vivier et al. (2004) and Tyler et al. (1997). Vertical ocean flow velocities are neglected and a thin-shell approximation is used which contains depth-integrated and conductivity-weighted horizontal flow and induced electric currents. The atmosphere and upper mantle are treated as insulators (Vivier et al., 2004; Parkinson and Hutton, 1989). The thin shell is allowed to include an underlying layer of conductive sediments. Therefore, a global sediment conductance map has been derived using the method described by Everett et al. (2003) and sediment thicknesses of Laske and Masters (1997). Using this approach, the radial component of the motionally induced primary poloidal magnetic field is calculated. The primary toroidal oceanic induced magnetic signals are not considered in this study, since these are confined to the oceans and cannot be measured from the outside. Nevertheless, the toroidal component couples with the large conductivity contrasts between the oceans and continents, which leads to the generation of secondary

poloidal magnetic signals along the oceanic shorelines (Dostal et al., 2012; Szuts, 2010). In this study, only the primary poloidal induced magnetic signatures are considered that directly originate from large-scale ocean global circulation and that can be recorded at both sea surface and satellite altitude.

According to Vivier et al. (2004), the induced electric currents in the horizontal plane can be expressed as an electric stream function ψ_e which leads to a scalar model equation derived from Ampere's Law and Ohm's Law:

$$\nabla \cdot \left(\Sigma^{-1} \nabla \psi_\mathsf{e}\right) = \nabla \cdot \left(\Sigma^{-1} F_z \int_h \sigma \boldsymbol{u}_\mathsf{H} \mathrm{d}z \right). \tag{1}$$

Here, h is the variable height of the thin shell according to the bathymetry, Σ is the depth-integrated conductivity, σ is the conductivity at a given point, F_z is the radial part of the Earth's ambient geomagnetic field and $\boldsymbol{u}_\mathsf{H}$ is the horizontal ocean flow velocity. F_z is derived from the POMME-6 Magnetic Model of the Earth and $\boldsymbol{u}_\mathsf{H}$ is prognostically calculated with OMCT. The induced magnetic field b_r is then calculated from the stream function ψ_e using spherical harmonic expansion:

$$b_r(\phi, \vartheta, r) = \sum_{j=0}^{j_\mathsf{max}} \sum_{m=-j}^{j} \frac{1}{2} \frac{\mu_0}{r} \psi_{jm} \left(\frac{a}{r}\right)^{j+1} (j+1) Y_{jm}(\phi, \vartheta). \tag{2}$$

Here, ϕ and ϑ are longitudinal and colatitudinal coordinates on the sphere, μ_0 is the permeability of free space, a is the Earth's radius, r is the height above sea level, ψ_{jm} and $Y_{jm}(\phi, \vartheta)$ are the spherical harmonic coefficients and functions. The spherical harmonic coefficients are calculated according to Driscoll and Healy (1994). In consequence of applying a spherical harmonic expansion, this approach gives the opportunity to easily calculate the motionally induced magnetic field at both sea level and satellite altitude. The ocean model's horizontal resolution of $1.875° \times 1.875°$ corresponds to a global grid size of 194×96 grid cells. In order to prevent aliasing effects that would otherwise occur during grid transforma-

tions, the maximum degree and order of the spherical harmonic expansion $j_{\max}$ is limited to $47 = \frac{96}{2} - 1$ (Driscoll and Healy, 1994).

2.3 Sea-water conductivity distribution experiments

The OMCT prognostically calculates ocean velocities, salt and temperature distributions at every time step (Thomas et al., 2001). The variables are subsampled and stored daily over the simulation period of one year. From OMCT salt and temperature values the sea-water conductivity is estimated using the transformation method from Apel (1987), resulting in 3-D spatio-temporal variable conductivity distributions.

In order to assess the influence of sea-water conductivity distributions on the motional induction process, three simulation experiments are performed. For all three experiments the motionally induced magnetic field is calculated using different distributions of sea-water conductivity, but from the same previously stored OMCT velocities and the same background magnetic field. For the first experiment ("constant conductivity experiment"), a globally uniform and constant in time mean sea-water conductivity of $3.5\,\mathrm{S\,m^{-1}}$ is applied at every grid point and every time step. For the second experiment ("spatially-variable-conductivity experiment"), the previously stored three dimensional and temporal variable conductivity distribution is processed. Annual mean values are derived from the conductivity distribution for every grid point, resulting in a 3-D variable but time-constant conductivity. For the third experiment ("spatio-temporal-variable-conductivity experiment"), the fully spatio-temporal variable conductivity distribution is utilized to calculate the induced magnetic fields.

3 Results and discussion

The annual mean global sea-water conductivity distribution at sea surface and two representative longitudinal depth-profiles is depicted in Figs. 1 and 2. Note, that this conductivity distribution exhibits both horizontal and vertical gradients, affecting the conductivity-weighting of the horizontal ocean velocities $\boldsymbol{u}_{\mathrm{H}}$ (see Eq. 1). Due to high temperature and salinity values, the highest values of up to $6\,\mathrm{S\,m^{-1}}$ occur in equatorial and some coastal

regions. A decrease of conductivity arises in poleward directions where lower temperature and salinity values occur. The depth profiles show that the least conducting areas are located in polar regions and lower parts of the ocean basin with values as low as $2.5\,\mathrm{S\,m^{-1}}$. In comparison to equatorial regions, depth-profiles in polar areas show an inverted conductivity gradient with lowest values in the upper ocean.

When using a globally uniform sea-water conductivity, the signals of the motionally induced magnetic field at sea level due to global ocean circulation range from -5 to 4 nT at sea level altitude. Mean values over the simulation period are in the range of -4 to 3 nT (Fig. 3). The local standard deviation reaches up to 10 % of the signal strength (Fig. 4). The strongest signals and variabilities occur in the area of the Antarctic Circumpolar Current (ACC). The characteristic separation into one positive part east of Australia and one negative part west of Australia are caused by the shape of the Earth's ambient geomagnetic field. Additional features are visible, e.g., the North Atlantic circulation and Western Boundary Currents along the eastern coasts of South Africa, South America or Japan. The results of the motionally induced magnetic field show good agreement with previous studies, e.g., Fig. 2 in Vivier et al. (2004) and Fig. 3 in Manoj et al. (2006). Vivier et al. (2004) compared motionally induced magnetic fields and their variability as calculated by three different ocean general circulation models (OGCM). For all three calculations, the same depth-integrated conductivity transport from one of the OGCMs is used. Manoj et al. (2006) utilized a mean sea-water conductivity of $3.2\,\mathrm{S\,m^{-1}}$ to calculate the exciting electric current in the ocean and a spatially-variable sea-water conductivity for modelling the shell conductance.

In order to assess the influence of the 3-D sea-water conductivity distribution on the variability of the magnetic signal, results from the constant conductivity experiment and spatially-variable-conductivity experiment are compared. Figure 5 shows the difference in the standard deviation of the magnetic signal, relative to the spatially-variable-conductivity experiment. Positive values indicate that using spatially variable conductivity profiles results in a larger temporal variability of b_r, whereas negative values state the opposite effect. Dominant positive areas are located in the zonal limits of 45° S and 45° N with values up to 45 %. The strongest negative areas, however, predominantly reside beyond 50° S and

50° N, reaching values up to −20 %. The most prominent positive features can be found in the Indian Ocean. Additional positive features are located in the area of the Kuroshio current, Agulhas current, east of Australia, along the equatorial jet in the Pacific Ocean, in the Gulf Stream and in the south Atlantic Ocean along the Brazil current. The signatures of the Western Boundary Currents can clearly be identified. Most prominent negative features are located in the area of the Aleutian Islands and the Antarctic Circumpolar Current. Note, that comparing the spatially-variable-conductivity experiment to other uniform conductivity distributions instead of $3.5\,\mathrm{S\,m^{-1}}$ will change patterns (especially zero-crossings) and strength of the values shown in Fig. 5. The result of a local under- and over-estimation still holds.

The high changes in temporal variability of the induced magnetic field and their spatial pattern are only partly explained by the horizontal conductivity distribution in the spatially-variable conductivity experiment (compare Figs. 1 and 5). Therefore, the difference between the depth-mean conductivity of the spatially-variable-conductivity experiment and the globally constant conductivity of the constant conductivity experiment are calculated. The differences are divided by the globally constant conductivity and illustrated in Fig. 6, showing the relative increase or decrease of the depth-mean conductivity at any point. The values reside in the range of ±60 % (peak to peak), whereas most changes reside in the range of ±20 %. An increase emerges in areas where the surface conductivity lies above the mean of $3.5\,\mathrm{S\,m^{-1}}$ and water-depth is comparably small. The largest decrease occurs in areas where the surface conductivity lies below the mean (see Figs. 2 and 6). Particularly, coastal regions and oceanic ridges form prominent features, e.g., Central Indian Ridge and East Pacific Rise. The comparison of the conductivity differences (Fig. 6) and changes in the variability of the magnetic field (Fig. 5) shows much more agreement than Figs. 1 and 5. Before the depth-integration over the water column according to the thin-shell approximation (Eq. 1), ocean flow velocities are multiplied by their specific conductivity. Consequently, ocean flow velocities are weighted by a comparably high conductivity in areas of positive changes in depth-mean conductivity or by a comparably low conductivity in areas of negative changes (see Fig. 6). This effect is visible around Indonesia, east of Australia in the

Pacific Ocean and in the north Atlantic Ocean (compare Fig. 5). Again, the general findings also hold for other globally uniform conductivities than $3.5\,\mathrm{S\,m^{-1}}$.

However, in areas where the most prominent changes in magnetic field variability arise, i.e., Indian Ocean, Aleutian Islands, mid Pacific Ocean and south Atlantic Ocean, only few significant changes in the depth-mean conductivity are visible. These discrepancies are explained by vertical gradients of the conductivity, together with near surface ocean flow velocities and their large temporal variability. Figures 7 and 8 show annual mean depth-integrated ocean flow velocities over the upper 1040 m and their standard deviation. The water column thickness of approximately one kilometer is chosen, since the largest deviations in conductivity from the mean occur in this layer (compare Fig. 2). In this layer, high ocean flow velocities and variability are weighted by an above-average conductivity in the areas of the Gulf Stream, Indian Ocean, mid Paficic Ocean (compare Figs. 2 and 8). This leads to an amplification of the magnetic field variability, although the depth-mean conductivity is similar to the globally constant conductivity used in the constant conductivity experiment. In addition, ocean currents are much more visible in the variability of the magnetic signal (see Figs. 4 and 5). Since the variability of the motionally induced magnetic signal distinguishes the oceanic contribution from the static crustal field, this is a key feature for the detection of global ocean flow in satellite data. The opposite effect occurs in high latitudes. In the Arctic Ocean, around the Aleutian Islands and in the Antarctic Circumpolar Current, high ocean flow velocities and variability in the upper layer are weighted by a below-average conductivity. Here, this leads to a relative dampening of the magnetic field variability.

In order to identify the influence of temporal variability of the conductivity distribution on motional induction, results from the spatially-variable-conductivity experiment and spatio-temporal-variable-conductivity experiment are compared. As opposed to the change of standard deviation induced by spatial conductivity gradients, only negligible differences are determined, which is based on the very small temporal variability of the conductivity distribution. The standard deviation does not exceed $0.7\,\mathrm{S\,m^{-1}}$ at the surface and $0.01\,\mathrm{S\,m^{-1}}$ below the upper 1040 m. Consequently, the influence of conductivity distributions on the

variability of motionally induced magnetic fields is predominantly driven by spatial contrasts of the conductivity.

4 Conclusion and summary

In order to model and simulate ocean circulation induced magnetic fields, a 2-D electromagnetic induction model is implemented into the ocean global circulation model OMCT. This combination gives the unique possibility to not only calculate motionally induced magnetic signals, but to assess the impact of oceanographic phenomena on the induction process. All necessary oceanic quantities for the estimation of ocean global circulation induced magnetic signals are calculated by the model. In this study, we focused on the question to what extent spatial and temporal variability in sea-water conductivity influences oceanic induced magnetic fields. Over the simulation period of one year, it is shown that assuming a globally uniform sea-water conductivity is insufficient in order to accurately capture the variability of the oceanic induced magnetic signal. Applying a three dimensional non-uniform conductivity distribution rather than a globally constant conductivity increases the temporal variability of the magnetic field up to 45 % in equatorial regions. In polar regions, a decrease of up to 20 % is detected. Hence, assuming an ocean-wide uniform conductivity leads to an underestimation of the variability of the motionally induced magnetic field in equatorial regions and to an overestimation in polar regions. These variations are only partly explained by horizontal gradients in the inhomogeneous sea-water conductivity distribution. The results show that especially vertical gradients in the conductivity distribution together with the bathymetry form a key feature for changes in the variability of the motionally induced magnetic signal. Ocean currents and their temporal variability in the upper ocean are amplified (dampened) in equatorial regions (polar regions) by the vertical conductivity structure and are, in turn, much more (less) visible in the induced magnetic signal. However, accounting additionally for temporally variable conductivity has negligible impact on the temporal variability of the magnetic field.

In past studies, different modelling approaches and parametrizations have been used to simulate global ocean induced magnetic fields. There is a consensus regarding the small variability of ocean induced magnetic fields and, consequently, its difficult detectability and separability from other magnetic signals in satellite data, e.g., in many regions, the crustal magnetic field has comparable or higher amplitudes in satellite measurements. The temporal variations of the oceanic induced magnetic field, however, distinguish it from the static crustal field. Thus, it is of particular importance to account for a realistic conductivity distribution in the ocean, in order to capture the temporal variability of the induction process more accurately, which may help future studies to more easily detect global ocean induced magnetic signals in satellite-based measurements.

Other approaches for modelling electromagnetic induction in the ocean might show a different response (in terms of patterns and strength) to a variable sea-water conductivity distribution. However, the principal effect of a variable sea-water conductivity should not be neglected in any model configuration. Therefore, the results of this study are not solely confined to magnetic fields that are induced by ocean general circulation and related studies dealing with motional induction in the ocean will also benefit from this paper. Subsequent studies should extend the findings of this study by investigating the contribution of a full 3D electromagnetic induction model. This would allow to assess the influence of vertical gradients in the sea-water conductivity distribution, which are only resolved by the thin-shell approximation in an integral sense. Additionally, a comparison between the influence of variable sea-water conductivity and a conductive mantle below the sediment layer could help to further quantify the interactions and aggregated effects of different conductivity structures and their effect on motional induction in the ocean.

Acknowledgements. This work has been funded by the Helmholtz graduate research school GeoSim. This study could not have been done without the supply of ERA-Interim data from the European Centre for Medium-Range Weather Forecasts and facilities from the German High Performance Computing Centre for Climate- and Earth System Research. Our spherical harmonic analyses were performed using the freely available software archive SHTOOLS (shtools.ipgp.fr).

The article processing charges for this open-access publication were covered by a Research Centre of the Helmholtz Association.

References

Apel, J. R.: Principles of Ocean Physics, vol. 38, International Geophysics Series, Academic Press, San Diego, California, 1987.

Chave, A. D.: On the theory of electromagnetic induction in the Earth by ocean currents, J. Geophys. Res., 88, 3531, doi:10.1029/JB088iB04p03531, 1983.

Chave, A. D. and Luther, D. S.: Low-frequency, motionally induced electromagnetic fields in the ocean 1. Theory, J. Geophys. Res., 95, 7185–7200, 1990.

Dee, D. P., Uppala, S. M., Simmons, A. J., Berrisford, P., Poli, P., Kobayashi, S., Andrae, U., Balmaseda, M. A., Balsamo, G., Bauer, P., Bechtold, P., Beljaars, A. C. M., van de Berg, L., Bidlot, J., Bormann, N., Delsol, C., Dragani, R., Fuentes, M., Geer, A. J., Haimberger, L., Healy, S. B., Hersbach, H., Hólm, E. V., Isaksen, L., Kaallberg, P., Köhler, M., Matricardi, M., McNally, A. P., Monge-Sanz, B. M., Morcrette, J.-J., Park, B.-K., Peubey, C., de Rosnay, P., Tavolato, C., Thépaut, J.-N., and Vitart, F.: The ERA-Interim reanalysis: configuration and performance of the data assimilation system, Q. J. Roy. Meteor. Soc., 137, 553–597, doi:10.1002/qj.828, 2011.

Dill, R.: Hydrological model LSDM for operational Earth rotation and gravity field variations, Tech. rep., Helmholtz-Zentrum Potsdam Deutsches GeoForschungsZentrum, Potsdam, Germany, doi:10.2312/GFZ.b103-08095, 2008.

Dobslaw, H. and Thomas, M.: Simulation and observation of global ocean mass anomalies, J. Geophys. Res., 112, C05040, doi:10.1029/2006JC004035, 2007.

Dostal, J., Martinec, Z., and Thomas, M.: The modelling of the toroidal magnetic field induced by tidal ocean circulation, Geophys. J. Int., 189, 782–798, 2012.

Driscoll, J. R. and Healy, D. M.: Computing Fourier transforms and convolutions on the 2-sphere, Adv. Appl. Math., 15, 202–250, 1994.

Everett, M. E., Constable, S., and Constable, C. G.: Effects of near-surface conductance on global satellite induction responses, Geophys. J. Int., 153, 277–286, 2003.

Faraday, M.: Experimental researches in electricity, Philos. T. Roy. Soc. A, 122, 125–162, 1832.

Flosadóttir, A. H., Larsen, J. C., and Smith, J. T.: Motional induction in North Atlantic circulation models, J. Geophys. Res., 102, 10353–10372, 1997.

Greatbatch, R. J.: A note on the representation of steric sea level in models that conserve volume rather than mass, J. Geophys. Res., 99, 12767, doi:10.1029/94JC00847, 1994.

Kuvshinov, A.: 3-D global induction in the oceans and solid earth: recent progress in modeling magnetic and electric fields from sources of magnetospheric, ionospheric and oceanic origin, Surv. Geophys., 29, 139–186, 2008.

Kuvshinov, A., Sabaka, T., and Olsen, N.: 3-D electromagnetic induction studies using the Swarm constellation: mapping conductivity anomalies in the Earth's mantle, Earth Planets Space, 58, 417–427, 2006.

Larsen, J. C.: Electric and magnetic fields induced by deep sea tides, Geophys. J. Roy. Astr. S., 16, 47–70, 1968.

Laske, G. and Masters, G.: A global digital map of sediment thickness, Eos T. Am Geophys. Un, 78, F483, 1997.

Manoj, C., Kuvshinov, A., Maus, S., and Lühr, H.: Ocean circulation generated magnetic signals, Earth Planets Space, 58, 429–437, 2006.

Parkinson, W. D. and Hutton, V. R. S.: The Electrical Conductivity of the Earth, vol. 3, Academic Press, San Diego, Calif., 261–232, 1989.

Sanford, T. B.: Motionally induced electric and magnetic fields in the sea, J. Geophys. Res., 76, 3476–3492, 1971.

Schnepf, N. R., Manoj, C., Kuvshinov, A., Toh, H., and Maus, S.: Tidal signals in ocean-bottom magnetic measurements of the Northwestern Pacific: observation versus prediction, Geophys. J. Int., 198, 1096–1110, 2014.

Stephenson, D. and Bryan, K.: Large-scale electric and magnetic fields generated by the oceans, J. Geophys. Res., 97, 15467–15480, 1992.

Szuts, Z. B.: Relationship between ocean velocity and motionally induced electrical signals: 2. In the presence of sloping topography, J. Geophys. Res., 115, C06004, doi:10.1029/2009JC006054, 2010.

Thomas, M., Sündermann, J., and Maier-Reimer, E.: Consideration of ocean tides in an OGCM and impacts on subseasonal to decadal polar motion excitation, Geophys. Res. Lett., 28, 2457–2460, doi:10.1029/2000GL012234, 2001.

Tyler, R. H., Mysak, L. A., and Oberhuber, J. M.: Electromagnetic fields generated by a three dimensional global ocean circulation, J. Geophys. Res., 102, 5531–5551, 1997.

Tyler, R. H., Maus, S., and Lühr, H.: Satellite observations of magnetic fields due to ocean tidal flow, Science, 299, 239–241, 2003.

Vennerstrom, S., Friis-Christensen, E., Lühr, H., Moretto, T., Olsen, N., Manoj, C., Ritter, P., Rastätter, L., Kuvshinov, A., and Maus, S.: The Impact of Combined Magnetic and Electric Field Analysis and of Ocean Circulation Effects on Swarm Mission Performance, Tech. rep., Danish National Space Center, Kgs. Lyngby, Denmark, 2005.

Vivier, F., Meier-Reimer, E., and Tyler, R. H.: Simulations of magnetic fields generated by the Antarctic Circumpolar Current at satellite altitude: Can geomagnetic measurements be used to monitor the flow?, Geophys. Res. Lett., 31, L10306, doi:10.1029/2004GL019804, 2004.

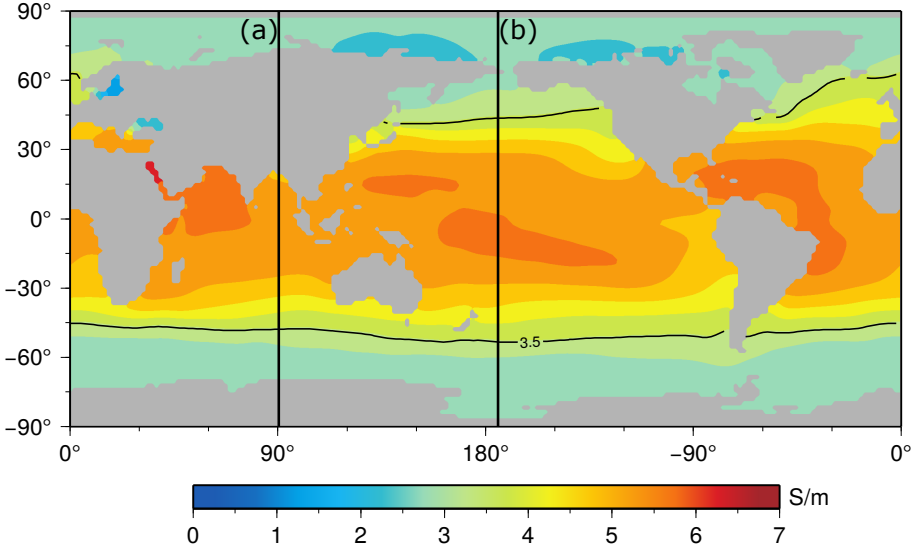

Figure 1. Annual mean sea-water conductivity of the upper ocean in $S\,m^{-1}$. The black meridional lines indicate the locations of the sections in the Fig. 2a and b. The black contour line indicates the mean conductivity of $3.5\,S\,m^{-1}$.

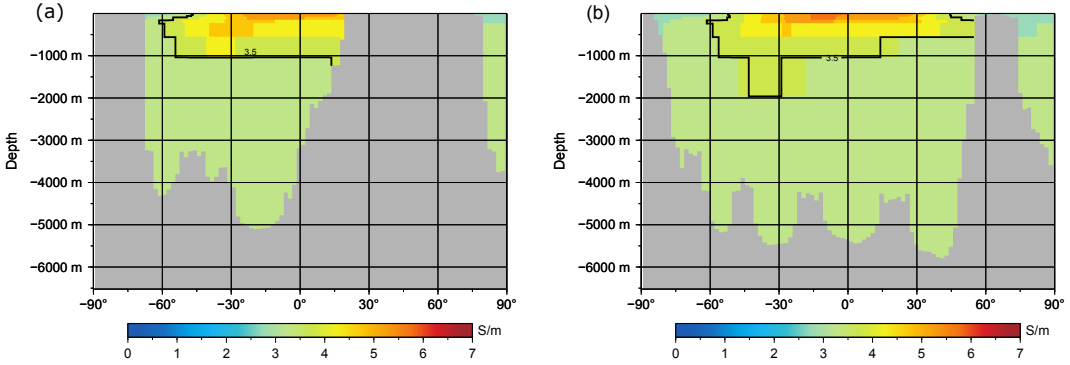

Figure 2. Meridional sections of sea-water conductivity distribution at 90° E **(a)** and 182° E **(b)**. Ocean depth is given in m. The black contour line indicates the mean conductivity of 3.5 S m^{-1}.

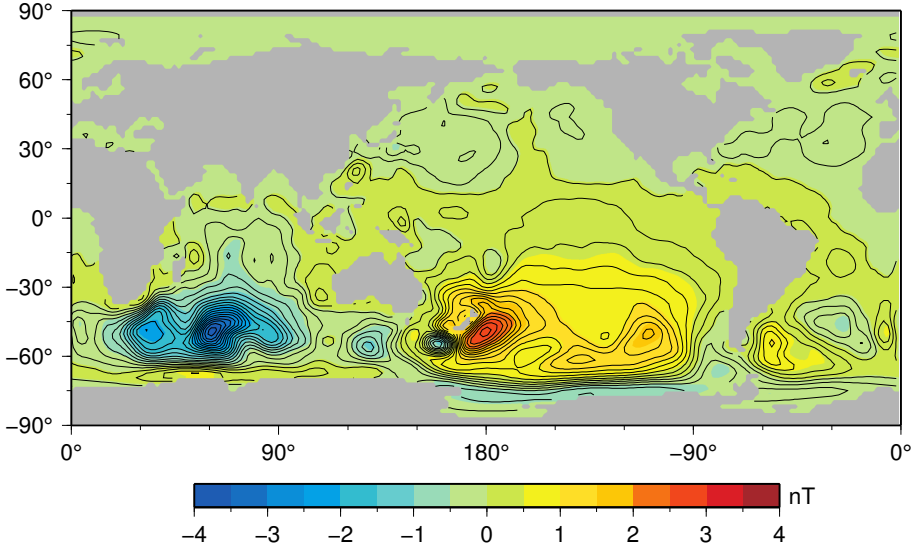

Figure 3. Annual mean values of motionally induced magnetic field at sea level altitude due to ocean global circulation from the constant conductivity experiment in nano Tesla (nT).

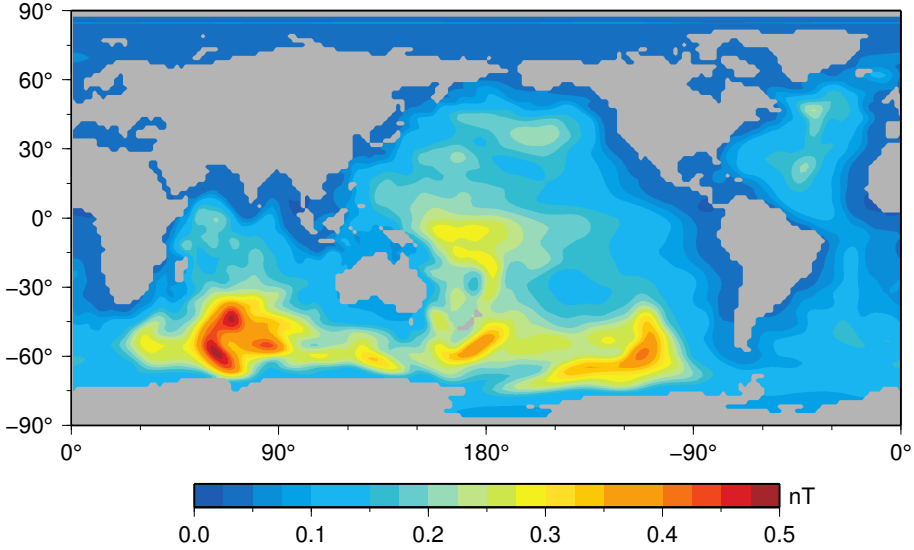

Figure 4. Standard deviation of motionally induced magnetic field at sea level altitude due to ocean global circulation from the constant conductivity experiment in nano Tesla (nT).

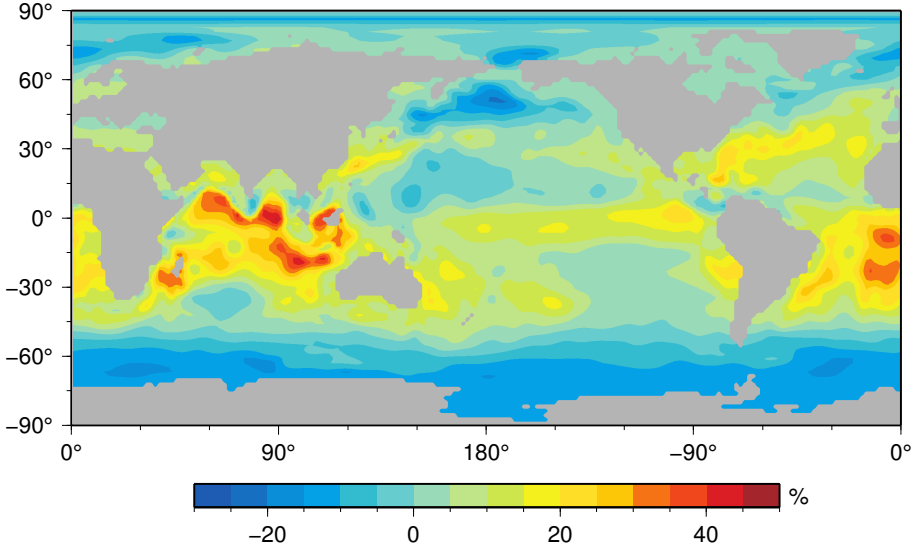

Figure 5. Influence of the spatially variable conductivity on the variability of the motionally induced magnetic field.

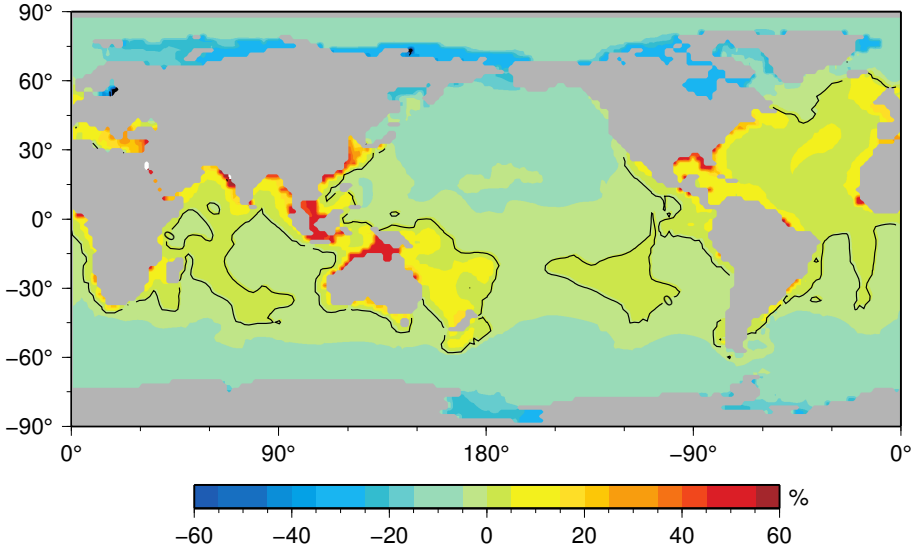

Figure 6. Relative difference between depth-mean conductivity used in the spatially-variable-conductivity experiment and globally constant conductivity of $3.5\,\mathrm{S\,m^{-1}}$ used in the constant conductivity experiment. The black contour line highlights the transition from positive to negative values.

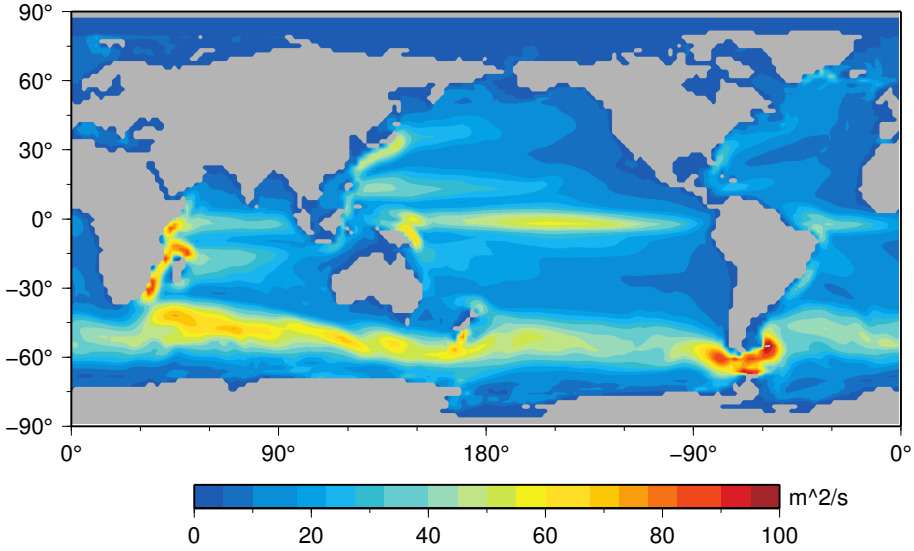

Figure 7. Annual mean depth-integrated ocean flow velocities over the upper 1040 m.

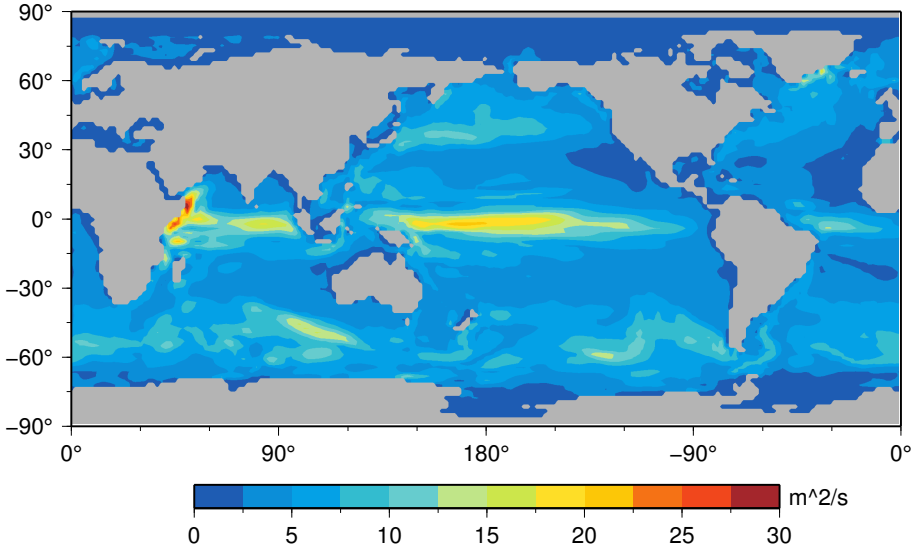

Figure 8. Standard deviation of depth-integrated ocean flow velocities over the upper 1040 m.